remote sensing

MDPI

Article

An Object-Based Approach to Extract Aquaculture Ponds with 10-Meter Resolution Sentinel-2 Images: A Case Study of Wenchang City in Hainan Province

Yingwen Hu [1,2,3], Li Zhang [1,2], Bowei Chen [1,2,*] and Jian Zuo [1,2,3]

[1] International Research Center of Big Data for Sustainable Development Goals, Beijing 100094, China
[2] Key Laboratory of Digital Earth Science, Aerospace Information Research Institute, Chinese Academy of Sciences, Beijing 100094, China
[3] University of Chinese Academy of Sciences, Beijing 100049, China
* Correspondence: chenbw@aircas.ac.cn; Tel.: +86-10-82178109

Abstract: Coastal aquaculture has made an important contribution to global food security and the economic development of coastal zones in recent decades. However, it has also damaged these coastal zones' ecosystems. Moreover, coastal aquaculture is poised to play a key role in the achievement of Sustainable Development Goals (SDGs). Consequently, extracting aquaculture has become crucial and valuable. However, due to the limitations of remote sensing image spatial resolution and traditional extraction methods, most research studies focus on aquaculture areas containing dikes rather than individually separable aquaculture ponds (ISAPs). This is not an accurate estimation of these aquaculture areas' true size. In our study, we propose a rapid and effective object-based method of extracting ISAPs. We chose multi-scale segmentation to generate semantically meaningful image objects for various types of land cover, and then built a decision tree classifier according to the unique features of ISAPs. The results show that our method can remove small rivers and other easily confused features, which has thus far been difficult to accomplish with conventional methods. We obtained an overall precision value of 85.61% with a recall of 84.04%; compared to the support vector machine's (SVM) overall precision value of 78.85% and recall rate of 61.21%, our method demonstrates greater accuracy and efficiency. We used this method to test the transferability of the algorithm to nearby areas, and the obtained accuracy exceeded 80%. The method proposed in this study could provide a readily available solution for the simple and efficient extracting of ISAPs and shows high spatiotemporal transferability.

Keywords: Hainan; aquaculture ponds; object-based; decision tree; Sentinel-2 image

Citation: Hu, Y.; Zhang, L.; Chen, B.; Zuo, J. An Object-Based Approach to Extract Aquaculture Ponds with 10-Meter Resolution Sentinel-2 Images: A Case Study of Wenchang City in Hainan Province. *Remote Sens.* **2024**, *16*, 1217. https://doi.org/10.3390/rs16071217

Academic Editors: Lin Yan, Juhua Luo and Ben Belton

Received: 25 January 2024
Revised: 21 March 2024
Accepted: 26 March 2024
Published: 29 March 2024

1. Introduction

Fishery resources are receiving increasing attention from a growing number of countries due to the challenges they face in the form of climate change, population growth, environmental degradation, land degradation, and the potential risks associated with genetically modified foods [1–5]. Since the growth of capture fisheries has become stagnant, fish stocks have become overexploited, and the global demand for protein continues to increase; aquaculture plays an important role in supplementing supplies of animal protein in various fishing industries [2]. Aquaculture production has grown rapidly over the past few decades [6]. In 2020, the worldwide COVID-19 pandemic brought about lockdowns and restrictions on movement, which hit the fishing industry hard [7]. Despite this setback, global aquaculture production is increasing, demonstrating that aquaculture has the potential to enhance the resilience of the global food system in the face of emergency. Aquaculture could provide a reliable source of food and employment, contributing directly to the Sustainable Development Goals (SDGs) of zero hunger (SDG2), no poverty (SDG1), and economic growth (SDG8) [8–11], particularly in developing countries. However, the rapid expansion

of coastal aquaculture [12–17] has resulted in significant competition for land [18]. This competition can cause direct and severe damage to coastal ecosystems, leading to environmental problems such as the shrinkage or disappearance of native coastal wetlands, water pollution, the destruction of natural habitats, the fragmentation of landscapes, the loss of biodiversity, and the increased vulnerability of coastal zones [19–23]. Competition for land is highly relevant to SDG14, which aims to protect oceans and marine resources.

Coastal aquaculture ponds are difficult to map due to their spectral similarity to other water bodies. Regarding the satellite data used for this task, Landsat satellites are a suitable option for monitoring large-scale aquaculture ponds due to their global coverage [12,14,24]. However, their low image resolution often makes it difficult to accurately detect dikes surrounding the ponds, resulting in low accuracy and high uncertainty. In contrast, high-resolution satellite image data (exemplified by China's Gaofen series and the American WorldView-2) have advantages in accurately extracting information on water bodies because they have proved able to overcome the influence of mixed pixels. Thus, their extraction results more closely resemble the actual area of the aquaculture pond in question [25–27]. However, their coverage is limited, making it difficult to map large areas of aquaculture ponds. Sentinel-1 imagery is increasingly used to map coastal aquaculture ponds due to its all-weather and day/night collection capabilities [28,29]. However, it has more speckle and boundary noise, both of which are challenging to suppress effectively and significantly reduce the signal-to-noise ratio and radiometric resolution [30]. In contrast, Sentinel-2 satellite images provide rich spectral information, high spatial resolution (10 m), and frequent temporal resolution (5 days of the revisit period) [31]. These features make them ideal for detecting dikes and characterizing seasonal changes in coastal aquaculture ponds, making them a valuable resource for mapping large coastal aquaculture ponds [32].

In recent years, several forms of algorithms have been researched for this purpose. The first such form is pixel-based methods [33]. Pixel-based methods involve identifying aquaculture and non-aquaculture pixels based on the spectral features of images. They are commonly used to extract aquaculture areas rather than ISAPs. However, their results often include dikes between neighboring ISAPs, causing ISAPs to merge with each other and resulting in the inaccurate sizing of the aquaculture area. The second such form is machine learning methods such as random forest and deep learning methods, which uses training samples [14,15,34,35]. Deep learning methods have been used extensively in aquaculture research. The U-Net network is widely used and has achieved good segmentation results [25,36,37]. However, when extracting large-scale aquaculture areas, these methods require numerous samples from various types of aquaculture areas [38]. The land cover datasets currently available to the public rarely include aquaculture ponds as a category. It is difficult to extract aquaculture areas when samples are lacking. Additionally, these models are essentially black boxes with poor interpretability, making it difficult to determine the cause of the problem and to improve and transfer methods. Moreover, recent research shows that deep learning methods can easily be fooled when the images' pixel values are subject to minimal perturbations. Such results mean they run the risk of making unexpected decisions. Better interpretability will help us to understand the rules used by the model to prevent potential unexpected situations [39]. Furthermore, these methods often require a complex combination of pre-processing and post-processing to obtain a reliable result, meaning they may be unsuited to the task of rapidly mapping large areas of aquaculture. The third is object-based methods [26,40–42]. Said methods first segment images to obtain objects composed of multiple neighboring pixels and then extract the aquaculture ponds based on their morphological features (such as the area, slope, and shape index) before establishing extraction rules for obtaining the aquaculture ponds. Compared with other methods, object-based methods of feature extraction are carried out on the object level to extract the features, and ISAPs within remote sensing images are represented as ponds of a more regular shape composed of multiple neighboring pixels. Object-based methods can extract their features more completely, avoiding the phenomena of fragmentation and

sticking. This method requires fewer samples, enabling mapping large areas of aquaculture ponds rapidly.

Existing studies have identified challenges in accurately extracting aquaculture ponds. The basic units of the aquaculture area are different individually separable aquaculture ponds (ISAPs). Unlike areas of ordinary agriculture, ISAPs in the same region have different fishing periods and closures, which can cause dry ISAPs to be mistaken for bare land in remote sensing images. This is a distinct feature that separates aquaculture from other types of agriculture. As aquaculture areas contain dikes and ISAPs represent individual pond scale, calculations of aquaculture production are more accurate when based on ISAPs rather than aquaculture regions. Many countries and national agencies lack the means to directly collect fishery data. Robust estimates of current and potential yields are essential for governments attempting to implement effective food security measures [43]. Therefore, the use of remote sensing images for extracting single ponds is a crucial development, particularly for countries with limited means of monitoring fisheries. Additionally, when disaster occurs, insurance companies need to assess the damage incurred, and it is more rational to calculate economic losses based on ISAPs. Wang mapped global aquaculture areas and compared them with the isolated ponds mapped by Ottinger and found that the difference in area between them is over 5000 km^2 within China, featuring an error of about 40% [33,44]. The extraction of ISAPs has therefore been proven to produce more meaningful results than the identification of clusters of aquaculture ponds, and it is more conducive to the accurate management of aquaculture areas.

Using Sentinel-2 imagery via the Google Earth Engine (GEE) platform, we developed an object-based decision method based on a comprehensive understanding of aquaculture ponds' morphological, spectral, and spatial characteristics. The results generated are expected to support the management of coastal aquaculture and facilitate the evaluation targets relevant to the SDGs. The objectives of this study are to select the most suitable water body index for the extraction of culture areas, to establish an ISAP extraction framework based on expert knowledge, and to compare the advantages and disadvantages of different algorithms.

2. Materials and Methods

2.1. Study Area

The proposed method was tested in a study area measuring 76.24 km^2 (110°43′43.59″–48′54.44″E, 19°44′10.98″–39′36.61″N, Figure 1a) located in Wenchang, Hainan Province, China. Wenchang City is the major aquaculture production area in Hainan. The study area is characterized by complex features, including many different water bodies such as rivers, puddles, and aquaculture ponds. Aquaculture ponds occupy a central region within the study area (Figure 1b), making the accurate extraction of aquaculture ponds quite challenging. The aquaculture ponds in the study area have the following characteristics. Firstly, most of the aquaculture ponds are clustered, being separated by dikes and surrounded by lakes. Next, the shapes and sizes of aquaculture ponds are varied. Moreover, the shape and size of the same ponds may not be fixed but change over time. Some ponds may shrink or even dry up due to harvesting periods. According to the *2021 China Fisheries Statistical Yearbook*, in 2020, Wenchang City accounted for 26.95% of Hainan Province's entire aquaculture area (the total area of mariculture and freshwater aquaculture in Hainan Province is 446.65 km^2). Therefore, we chose this area to test our proposed method and provide insight that will aid the scientific management of aquaculture in Hainan.

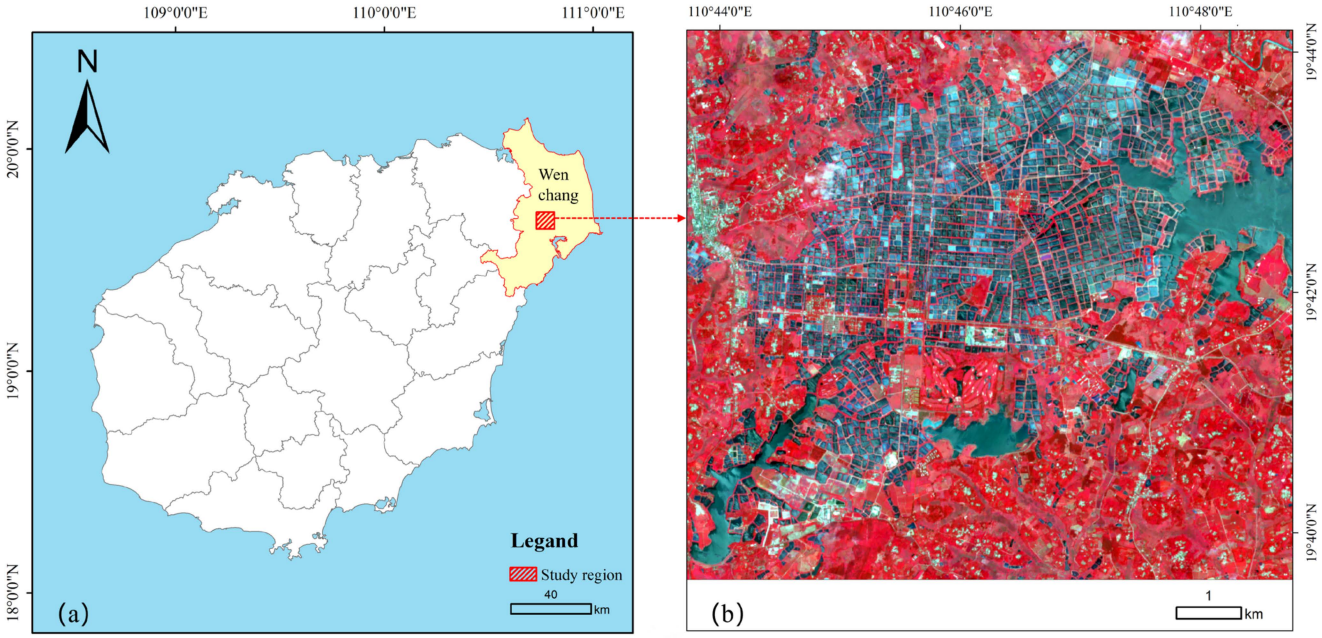

Figure 1. A map of the study area. (**a**) The location of the study region; (**b**) an overview of the study area (Sentinel-2 images; the band combination is 843).

2.2. Data

In this paper, we used Sentinel-2 multi-spectral images from 2022 to extract ISAPs. All images are Level-2A, and the cloud was removed based on the quality assessment (QA) band (for each image, low-quality observations due to clouds were masked using the QA60 bitmask band, and the remaining pixels were reserved, deemed good-quality observations). Each scene has spectral bands with 10 m spatial resolutions. Using time series data throughout the year can alleviate the problems caused by missing images resulting from cloud cover. It can also facilitate the extraction of aquaculture ponds during different harvesting periods. Due to the dynamic nature of aquaculture ponds, one or more ponds may run out of water or change location during the year. As a result, features from the same location within remote sensing images may be inconsistent, making it difficult to establish an accurate feature recognition model. To address this issue, we used the temporal aggregation function of GEE. All available high-quality pixels from Sentinel-2 multi-spectral images for the time series from January 2022 to December 2022 were composited into a single image by calculating the median of all values at each pixel across the stack of all bands. We thus obtained a high-quality composite image for 2022.

The above data extraction and data processing procedures are all completed on GEE, which is a remote sensing cloud computing platform launched by Google (https://earthengine.google.com).

2.3. Method

Extracting ISAPs from environments with complex surfaces is a challenging task. In terms of image segmentation, the inconsistent pixels and blurred boundaries of each aquaculture pond hinder the accurate segmentation of aquaculture ponds. Furthermore, aquaculture ponds vary in shape and size, making it difficult to correctly differentiate aquaculture ponds from other water objects. To confront the challenge of the large-scale and accurate extraction of individual aquaculture ponds, we propose an object-based method of aquaculture pond extraction. As shown in Figure 2, our process includes phases 1, 2, 3, 4, and 5, as follows. Phase 1: we removed clouds from the images and synthesized a median composite image for the whole year of 2022; Phase 2: Using multi-scale segmentation, we segmented the image into multiple objects. Although the shapes

and sizes of aquaculture ponds are different, all pixels in a single aquaculture pond are of similar brightness, and the difference in brightness between it and its surrounding features is significant. This means we can use multi-scale segmentation and use the ROC-LV curve to find the optimal segmentation scale; Phase 3 and 4: We constructed a decision tree based on the aquaculture sample data provided by manual visual interpretation and prior aquaculture knowledge. We did so according to the specific features of the aquaculture ponds; Phase 5: we performed an assessment of accuracy to eliminate obvious errors from the coastal aquaculture ponds.

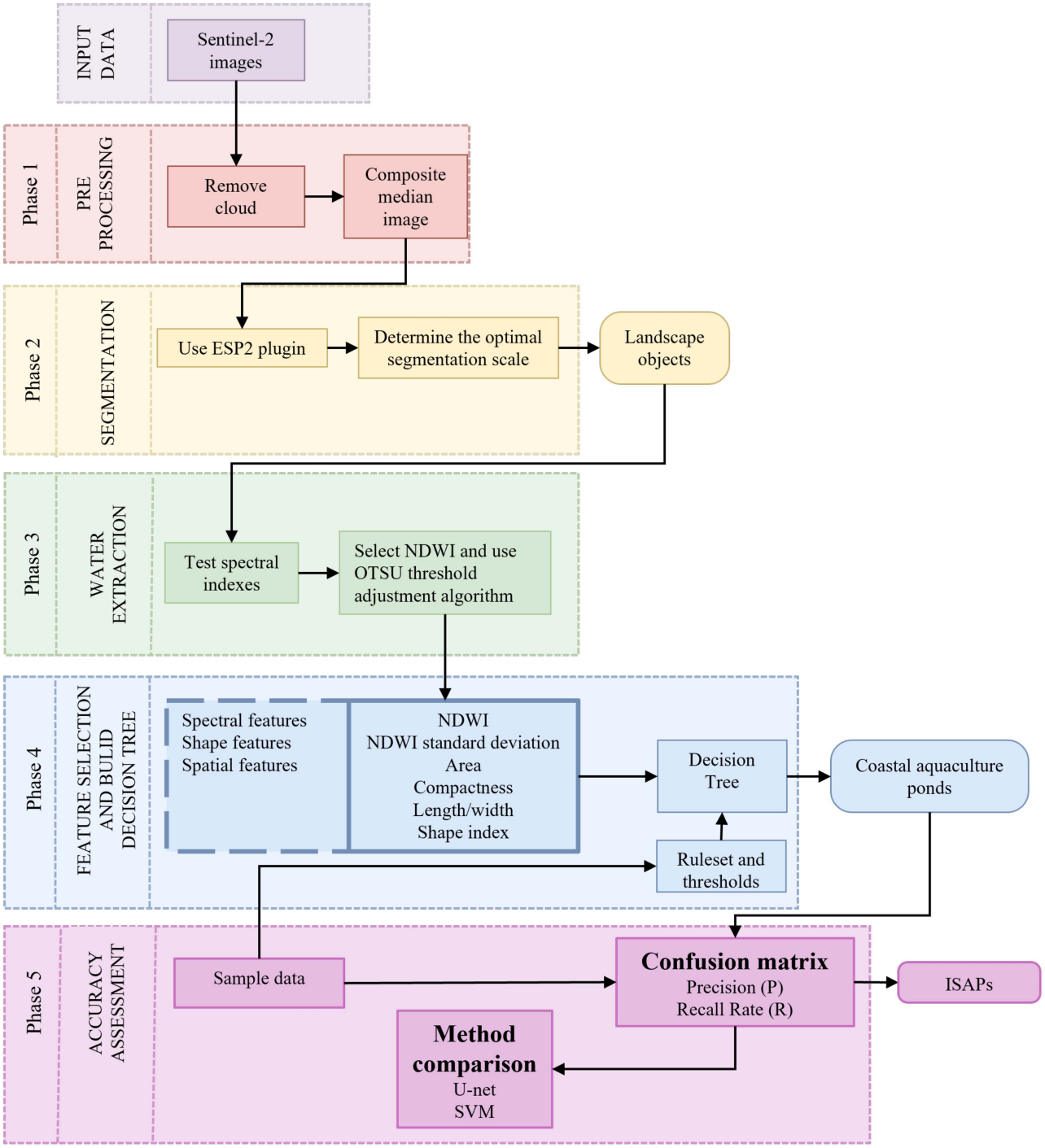

Figure 2. The overall workflow of the proposed methods for individually separable aquaculture pond (ISAP) extraction.

2.3.1. Generating Objects via Segmentation

Image segmentation is the first step of object-based methods, and segmentation directly determines the accuracy of the final classification results. There are various segmentation algorithms, such as edge-based algorithms [45–47], the Simple Linear Iterative Clustering (SLIC) super pixel algorithm [48–50], Multiresolution Segmentation (MRS) [51], and hybrid segmentation [52]. Different segmentation algorithms are applied to different scenarios and have their advantages and disadvantages. This paper will use multi-scale segmentation to segment the images of the study area. Multi-scale segmentation is based on the principle of minimizing regional heterogeneity. That is, the inhomogeneity between neighboring image units in one or more images is maximized at a specific segmentation scale threshold [53–56]. Multi-scale image segmentation can address some of the deficiencies associated with single-scale segmentation in environments with complex land cover [57].

In order to find the optimal segmentation scale most efficiently and avoid the influence of human factors on segmentation accuracy, the ESP2 plug-in in eCognition was used to determine the optimal segmentation scale. Drăguț et al. developed the Estimation of Scale Parameter (ESP) tool to detect optimal scales and proposed the rate of change of the local variance (denoted the rate of change in Figure 3) measures the change in LV from one object level to another. Thus, the most obvious peaks that dominate their neighborhood can be selected as indicators for optimal scale [58]. Drăguț et al. extended this approach into an automated tool (ESP2) for multiple layers and proved this tool consistently performed better than any of the randomly generated segmentations [59]. The eCognition 9.0 software is used to perform initial multi-scale image segmentation. As shown in Figure 3, the horizontal coordinates represent the segmentation scale parameters, and the vertical coordinates represent the local variance LV (red) and the rate of change ROC of the local variance (blue), respectively. Using the local peak of the ROC as the reference for the optimal segmentation scale, we selected five alternative scales (37, 64, 95, 114, and 122) marked by the yellow circles in Figure 3. The local effects of segmentation at different scales are shown in Figure 4. We observed optimal results with a segmentation scale of 37, where the ponds were not fragmented.

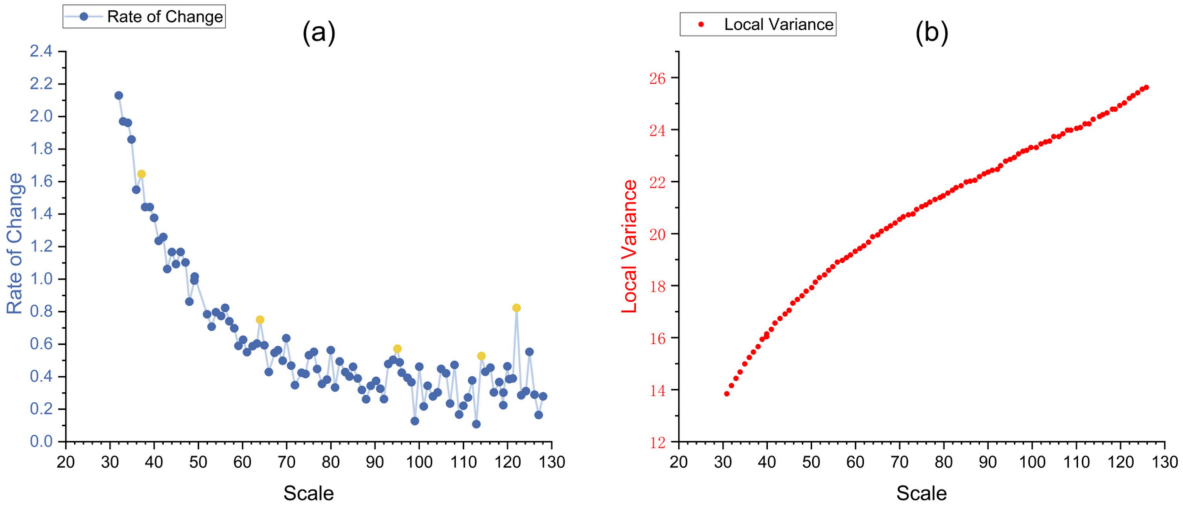

Figure 3. (**a**) Rate of change in image segmentation scale; (**b**) local variance in experimental area.

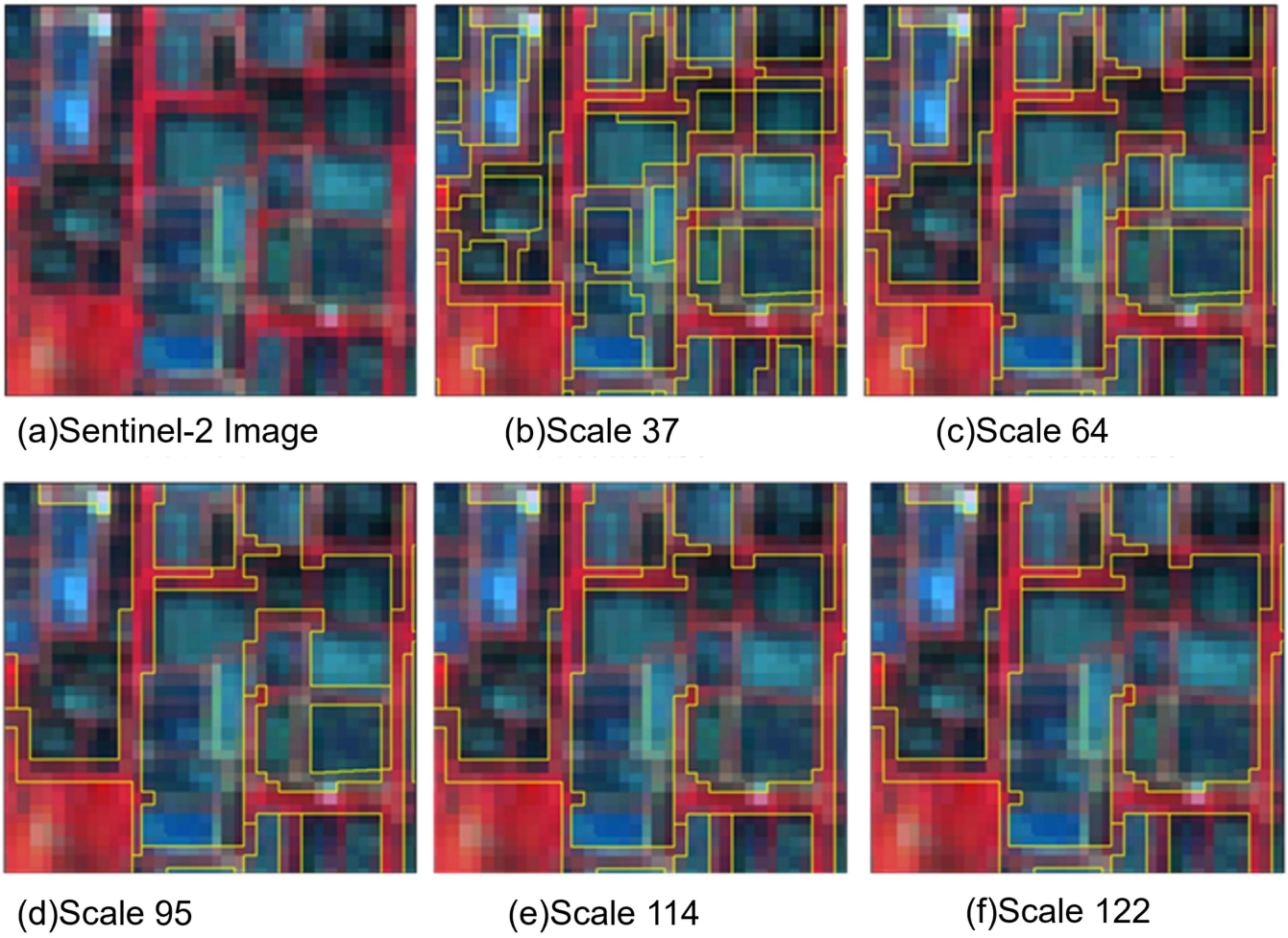

Figure 4. Different segmentation results.

2.3.2. Water Body Extraction Using Water Indices

Water bodies have more apparent differences from other features in terms of their spectral characteristics; these manifest as differences in brightness within remote sensing images. Index-based methods divide ground objects into the categories of water and non-water through band operation and threshold segmentation, which are the most convenient and widely used methods [60–62]. As a more specific kind of water body, aquaculture water bodies usually feature additional feed, farming drugs, and other substances, all of which will affect the water quality of the water body, resulting in higher sediment and organic matter contents. Said contents distinguish aquaculture water bodies from ordinary water bodies, and these differences are expressed as differences in reflectance characteristics within remote sensing images. This means a more suitable index can be selected to extract aquaculture water bodies according to their reflectance characteristics.

Currently, the most commonly used methods of extracting water bodies include single-band, dual-band, and multi-band methods. Herein, we analyzed and compared single-band, dual-band, and multi-band processes to choose the most suitable index for extracting aquaculture water bodies.

The basic tenet of the single-band method is using the difference in reflectivity between water and other pixels in a single band to identify areas of water; for example, water bodies in the near-infrared band have more noticeable differences [63].

Dual-band methods include the band ratio method and the normalized difference water index method [64]. The principle of the band ratio method is to use the ratio relationship between different bands in remote sensing images to distinguish different

feature types. The ratio is usually constructed by analyzing the target feature's strongest and weakest reflectance bands to expand the difference between the target and background features [65].

Our study area was divided into three categories, with approximately 14,000 sample pixel points selected for each category (aquaculture water bodies, non-aquaculture water bodies, and non-water bodies). We analyzed the distribution of the planted area and other features in the grayscale of each band, as shown in Figure 5.

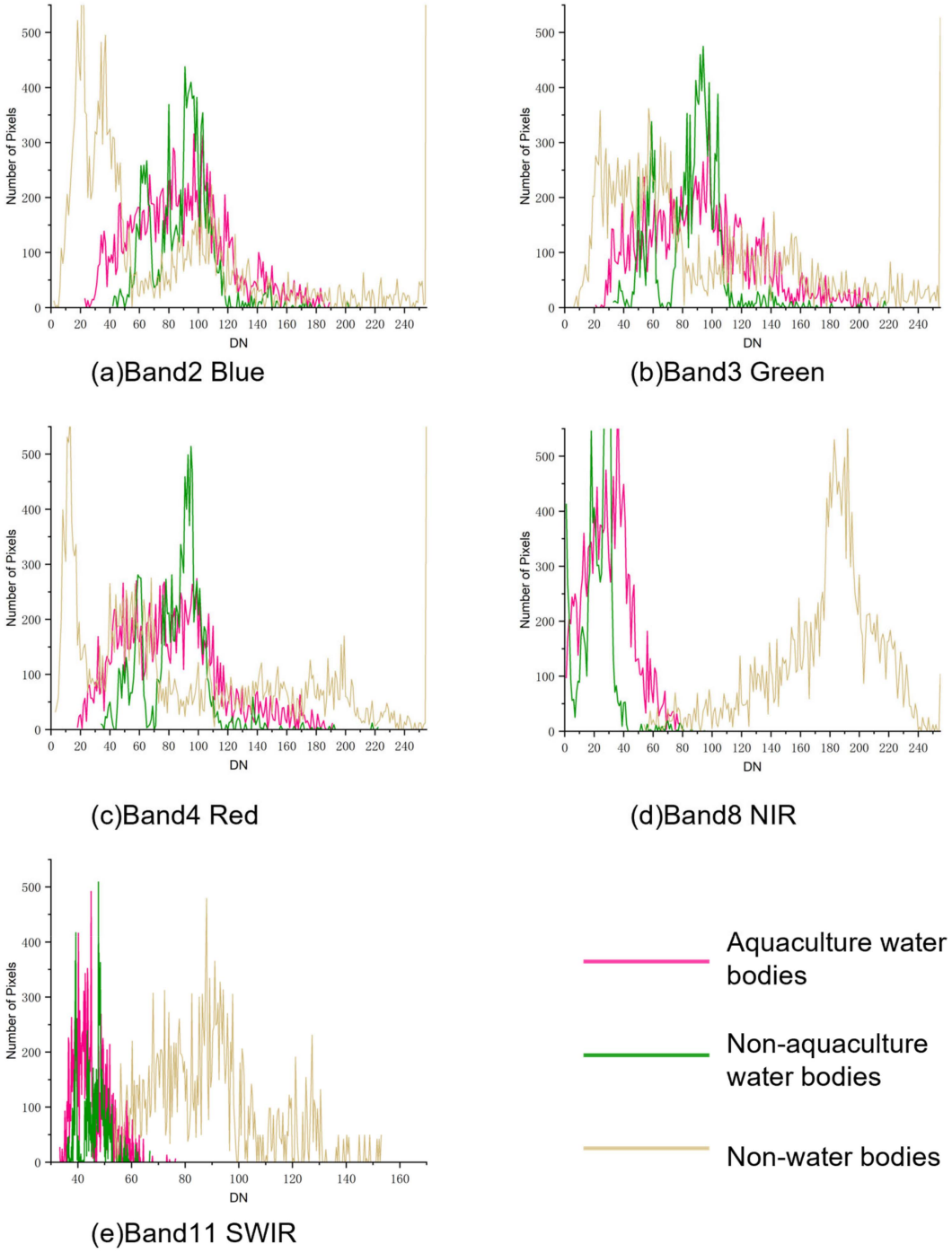

Figure 5. Distribution of grayscale values of aquaculture water bodies, non-aquaculture water bodies, and non-water bodies.

Figure 5 shows that the spectral differences between water bodies and non-water bodies are more evident in bands 8 and 11, so the single-band method led to the selection of these two bands and the subsequent construction of a dual-band index.

To address the problem that non-water features (e.g., soil and terrestrial vegetation) in the image may not be properly removed (McFeeters, 1996), multi-band methods have been developed. For example, the normalized difference water body index (NDWI) proposed by McFeeters in 1996 uses the normalized ratios of green and near-infrared (NIR) bands to depict water body features. The raw normalized difference water index (NDWI) is calculated as (green band − NIR band)/(green band + NIR band) [66]. In order to suppress the noise in built-up areas, another water body index, the MNDWI, was proposed. This index is based on the NDWI by replacing the NIR band with the short-wave infrared (SWIR) band [67]. The MNDWI can significantly enhance the contrast between areas of water and built-up areas by using (green band − SWIR band)/(green band + SWIR band). In addition, there is the method of the coma cap transformation of Sentinel-2 images proposed by Nedkov et al. [68], which orthogonalizes the raw data (including the brightness component, greenness component, wetness component, etc.) and transforms them into a multidimensional space. In this paper, we used one of the wetness components to extract the water bodies, herein referred to as WET.

We selected the seven indices mentioned above for the extraction experiments of the cultured water bodies, and the selected indices and expressions are shown in Table 1. After obtaining the grayscale images of each index, we used the Otsu threshold adjustment algorithm to test the extraction effect of different water indexing methods on the aquaculture water's surface [69–72]. This method is based on the maximum variance theory. It uses a threshold that minimizes the within-class variance to divide all the pixels in the image into two groups: target pixels and background pixels [73]. Then, we tested the missed ratio and the misclassification ratio of each index separately. Finally, we adopted the optimal index for extracting the water body.

Table 1. Water body extraction formula and band.

	Index	Formula	Band Type
Single-Band	B8	B8	NIR
	B11	B11	SWIR
Dual-Band	A1	B8/B3	NIR, Green
	A2	B11/B3	SWIR, Green
Multi-Band	NDWI	(B3 − B8)/(B3 + B8)	NIR, Green
	MNDWI	(B3 − B11)/(B3 + B11)	SWIR, Green
	WET	0.0649 × B1 + 0.1363 × B2 + 0.2802 × B3 + 0.3072 × B4 + 0.5288 × B5 + 0.1379 × B6 − 0.0001 × B7 − 0.0807 × B8 − 0.0302 × B9 − 0.4064 × B11 − 0.5602 × B12 − 0.1389 × B8A	Coastal aerosol, Blue, Green, Red, Vegetation red edge, NIR, Water vapor, SWIR, Narrow NIR

2.3.3. Establishing Classification Rule Sets

We used spectral features, spatial features, and shape features of objects to establish sets of classification rules. Spectral features were used to coarsely extract aquaculture ponds, removing most non-water objects. Shape and spatial features were used to distinguish aquaculture ponds from other water surfaces showing similar reflectance patterns and the dikes adjacent to the aquaculture ponds.

2.3.4. Extraction Method

In this study, we used the decision tree algorithm to extract ISAPs and compared it with the SVM and U-Net algorithms. In terms of feature space selection, both SVM and U-Net only use three bands in the image (NIR, Red, and Green).

The decision tree forms a hierarchical decision ruling structure by gradually segmenting the characteristics of remote sensing data. The decision tree algorithm is easy to

understand and explain; it can be analyzed visually, and rules can be extracted easily. This method is well suited to using remote sensing data to classify ground objects, identify coverage types, and monitor environmental changes. Because it is intuitive, easy to understand, and highly explainable, it is commonly applied in the field of remote sensing. Explainability helps to identify errors or biases in extraction results. It is easier to improve and transfer the method once there is a comprehensive understanding of the inner workings of the method and the full utilization of band information. In addition, in long-term or repeated applications, explainable methods are easier to maintain and update and can more easily respond to changes in data, technological advancements, and other changes in order to ensure the sustainability of the method. This is important for long-term observation and mapping projects. Explainability makes results easier to understand and trust. Decision makers and stakeholders are more likely to accept results that they can understand, which will encourage the acceptance and use of extraction methods.

The core idea of support vector machines is to find an optimal hyperplane that can separate samples of different categories. When data are not linearly separable, SVMs can map the original feature space to a high-dimensional feature space through kernel techniques to identify a better segmentation hyperplane. Concerning kernel functions, the radial basis function (RBF) kernel is the most effective and commonly used parameter in remote sensing image classifications [74]; we adopted it for this reason. The performance of the SVM model using the RBF kernel is greatly influenced by the values assigned to the two important parameters: C (penalty value) and γ (gamma). Therefore, to obtain the optimal values for these parameters, we conducted many experiments. We began the experiment with the following initial values: penalty value (C) = 50 and gamma = 0.01. Then, we performed 20 tests by gradually changing the value of C from 50 to 1000 in steps of 50 to obtain the best C value, while keeping γ and other values unchanged at the default value. After determining the optimum value of C, we conducted 10 tests to determine the best γ from a range of values (0.1, 0.2, 0.3, 0.4, 0.5, 0.6, 0.7, 0.8, 0.9, and 1.0) by fixing the best C value and using default values of other parameters. Finally, the two best values were selected to build the best SVM model.

The U-Net model is an improved FCN semantic segmentation model proposed in 2015 [75], which adopts a typical encoder–decoder structure and subscribes to the principle of FCN for the full convolutional semantic segmentation of images, incorporating the characteristics of jumping networks. It is very clever in structure and named because it follows U-shaped symmetry. We used Sentinel-2 images covering the study area to create a dataset. Based on ArcGIS10.8 software and Google HD images, we used visual interpretation to complete the manual annotation of breeding ponds in the study area. The Id value was set to 255 and given the binarized sample label. Because directly inputting the entire image and label into the model for training will cause the computer's memory to overflow, we used random cropping to crop the images, resulting in a Sentinel-2 image dataset of 750 images, which was then divided into a training set and a verification set according to a ratio of 8:2. Additionally, we performed data enhancement operations on the training set (including geometric transformations, such as horizontal flipping and vertical flipping, and brightness enhancement and contrast enhancement). We selected 20% of the expanded training set to act as a verification set for adjusting model parameters.

3. Results

3.1. Water Body Extraction with Water Indices

Here, we selected the best water body index, NDWI, by comparing the missed ratio and misclassification ratio of seven water body indices. The grayscale image of each index is shown in Figure 6.

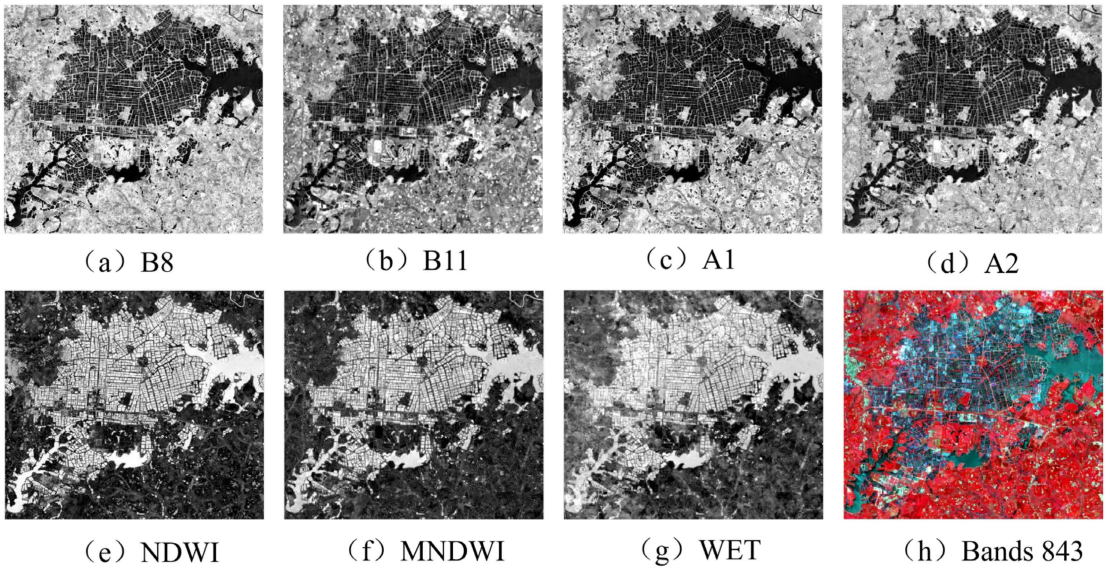

Figure 6. Grayscale images obtained with different indices.

According to the Otsu method, used to determine the optimal threshold value for each index grayscale image, the extraction results of each index used to extract the aquaculture region were obtained and are shown in Figure 7.

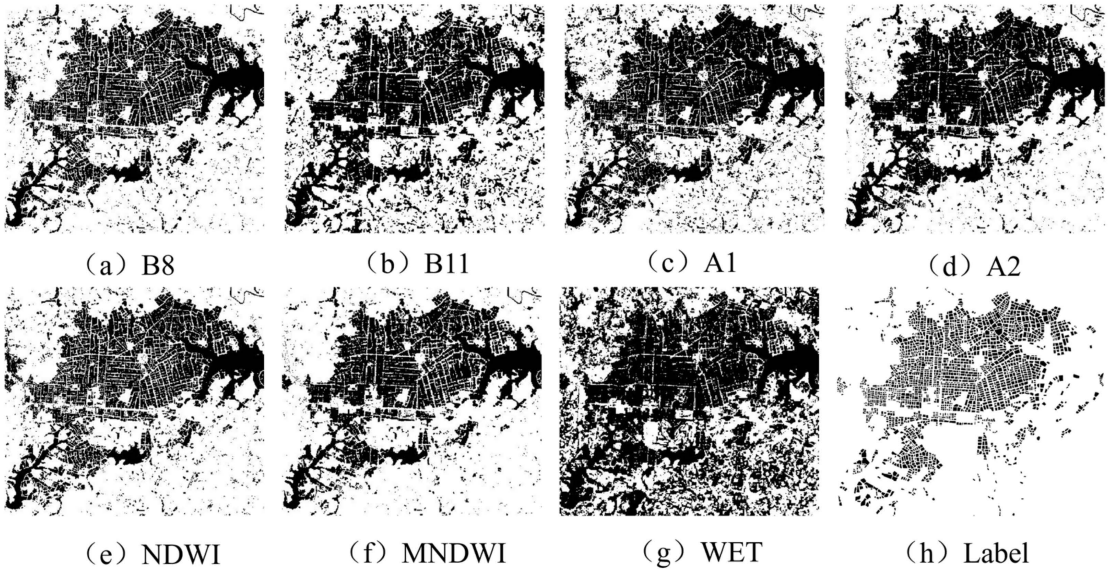

Figure 7. Aquaculture areas were extracted from each index, and the black pixels indicate extracted aquaculture ponds. Based on ArcGIS 10.8 software and Google HD imagery, visual interpretation was used to obtain the label of the aquaculture ponds in the study area.

It is observed that B8 within the single-band method and the NDWI and MNDWI (of the water body index methods) had better extraction effects compared with other methods. They extracted the water body more accurately. Labels drawn via visual interpretation were used as the standard to count the wrong and missing scores of these seven indices, and the results are shown in Table 2.

Table 2 shows that the proportions of wrong and missed scores are the smallest for the NDWI, followed by the two indices B8 and MNDWI. Accordingly, the NDWI was selected as the water body index used to distinguish between water body objects and non-water body objects.

Table 2. Wrong and missing scores for each index extraction result.

Index	Missed Ratio	Misclassification Ratio
B8	0.28%	18.59%
B11	0.52%	27.15%
A1	0.06%	26.22%
A2	0.27%	22.99%
NDWI	0.20%	18.47%
MNDWI	0.65%	18.49%
WET	0.44%	43.10%

3.2. Feature Selection for Aquaculture Ponds

By selecting aquaculture ponds and easily misclassified features such as dikes, rivers, and ponds on the island of Hainan, we found that aquaculture ponds have obvious differences from other features in terms of their area, compactness, length/width, NDWI standard deviation, and shape index, as shown in Figure 8. Therefore, within our object-based classification approach, these features were selected as the classification features of the object, and the details of the features are given in Table 3.

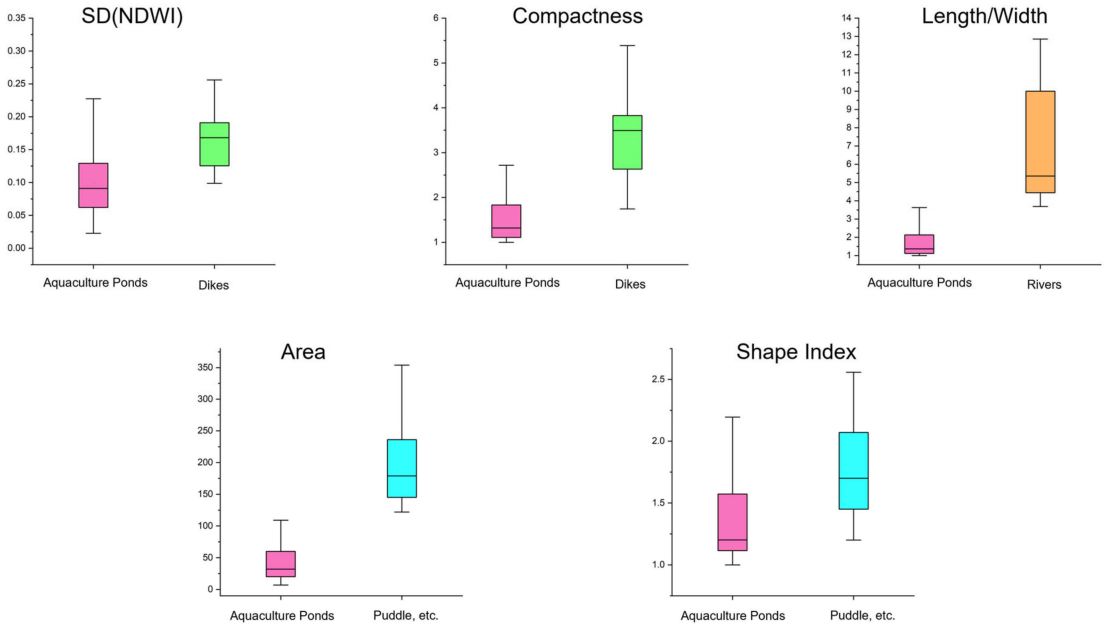

Figure 8. Various characteristic feature values among aquaculture ponds and others.

Table 3. Introduction of each feature.

Feature	Introduction
NDWI standard deviation	The standard deviation of NDWI values is calculated for all image elements of the image object, which reflects the dispersion of NDWI values. NDWI standard deviation = $\sqrt{\frac{\sum_{i=1}^{n}(NDWI_i - NDWI_{mean})^2}{n-1}}$
Area	The area of an object in the image without georeferencing is the number of image elements that make up the object, and the area of an object in the image with georeferencing is the true area of the image elements multiplied by the number of image elements of the object, and the image object in this paper has georeferencing, and the site is measured in metric acres.
Compactness	Compactness is the value obtained by multiplying the length and width of an image object and dividing it by the number of pixels in the object. Compactness = length × width/the number of pixels
Length/width	The aspect ratio is the ratio of the length and width of the object and is generally calculated from the approximate border.
Shape index	The shape index is four times the square root of the area of the image object multiplied by the length of its boundary. Shape index = $4 \times \sqrt{area}$ × the length of its boundary

3.3. Extracting Coastal Aquaculture Pond Objects Using Decision Trees

As shown in Figure 9, the mean (NDWIobject) represents the mean NDWI value of the image object, OTSU (NDWIarea) represents the NDWI threshold value determined according to the OTSU thresholding method in the study area, SD (NDWIobject) is the standard deviation of the NDWI of the image object, and the area is measured in metric acres. Firstly, the images are multi-scale segmented, and then the image objects are divided into water body objects and non-water body objects according to OTSU. This is the initial phase of differentiation between water bodies and non-water bodies; the vast majority of the water body objects are water bodies, but they still contain dikes and other misclassified features. Dikes can then be removed according to their NDWI standard deviation and compactness parameters, and adjacent objects are merged. Rivers can be well distinguished from aquaculture ponds by utilizing the aspect ratio feature. Finally, ponds, small spots, and some irregular misclassified features are removed by utilizing the parameters of area and shape index.

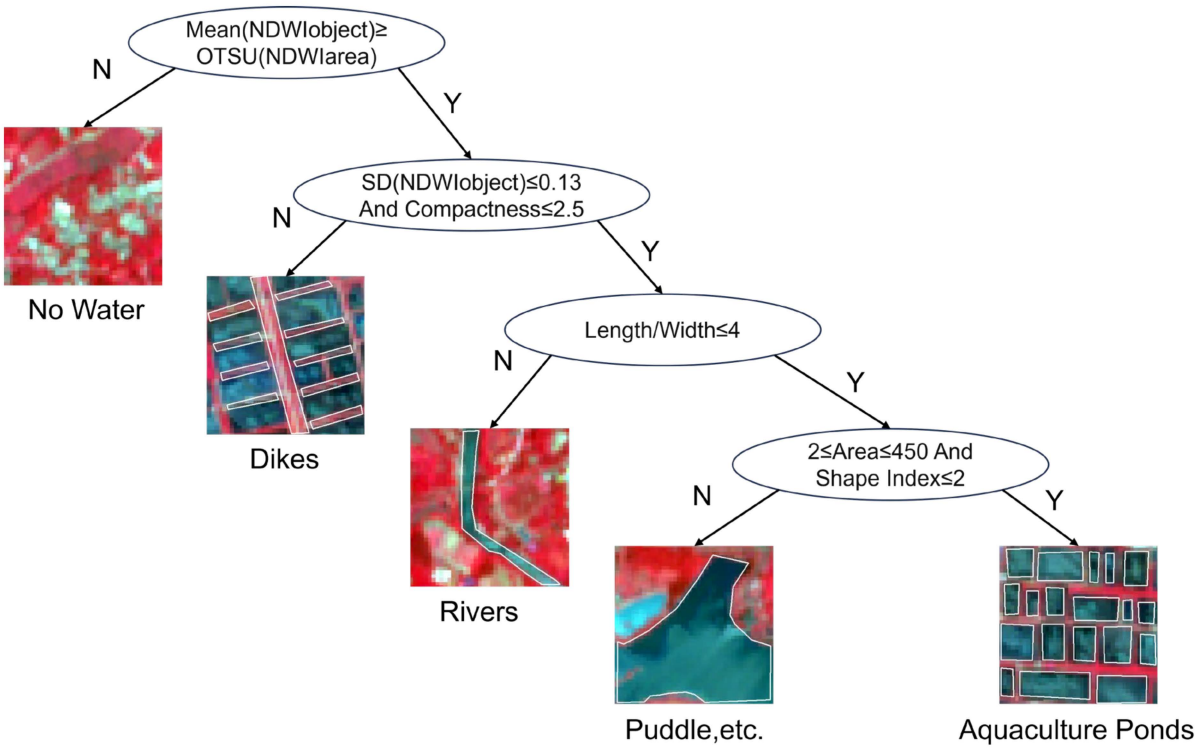

Figure 9. Decision tree for extracting aquaculture ponds.

3.4. Accuracy Assessment

To evaluate the strengths and weaknesses of our proposed method in terms of accuracy and overall extraction effectiveness, we compared the method with traditional machine learning methods, including SVM and deep learning methods (U-Net).

For the evaluation of precision, the results of manually drawn culture ponds were taken as reference samples for evaluating the accuracy of the extraction effects of the three methods. The confusion matrix-based evaluation indices precision (P) and recall rate (R) were used to quantitatively evaluate the accuracy of the three methods in extracting aquaculture ponds.

A confusion matrix of the real case and the extraction results is shown in Table 4. Aquaculture ponds are positive cases, and non-aquaculture ponds are negative cases.

Table 4. Confusion matrix table.

Confusion Matrix		Extraction Result	
		Positive	**Negative**
Label	Positive	TP	FN
	Negative	FP	TN

Precision (P) represents how many of the classes we predicted to be positive are actually positive:

$$P = \frac{TP}{TP + FP} \quad (1)$$

The recall rate (R) represents how many classes we correctly predicted among all the positive classes:

$$R = \frac{TP}{TP + FN} \quad (2)$$

Table 5 shows that the precision (P) and recall (R) of the object-based + decision tree method of extracting aquaculture ponds from Sentinel-2 remote sensing images are around 85%, while the recall (R) of the machine learning classification method is below 70%. The deep learning method achieved a precision (P) of 86.36% and a recall rate of 90.77%. Compared with the other two methods, SVM is the lowest in terms of precision (P) and recall (R), and the deep learning method is slightly better than this method in terms of precision (P) and about 6% higher than our method in terms of recall (R). From the comparison of the accuracy of the two extraction methods in Table 5, it is obvious that the object-based + decision tree method is better than the SVM method in terms of accuracy metrics across the board, but it is slightly inferior to the deep learning method.

Table 5. Precision and recall rate of extracted results via different methods.

	Machine Learning SVM	**Deep Learning (U-Net)**	**Object-Based + Decision Tree**
P/(%)	78.85	86.36	85.61
R/(%)	61.21	90.77	84.04

The details of the three methods' extraction effects are shown in Figure 10. Through comparative observation, we found that the extraction results of the SVM method have missed areas. Its extraction results are more fragmented, and the merging between different ponds is more significant. Thus, this method cannot extract individual aquaculture ponds accurately. The deep learning method can extract individual aquaculture ponds more effectively, and its extraction results are more complete, being that they lack fine impurities. That said, there are also some missed areas. The object-based + decision tree method reduced the number of missed areas, and its extraction process resulted in aquaculture ponds without the impurity patches that we observed when using the SVM method. In addition, this method proved to alleviate the phenomenon of adhesion between different aquaculture ponds and accomplished the accurate extraction of individual aquaculture ponds.

The overall extraction effect is shown in Figure 11. Both the deep learning and SVM methods failed to completely remove the fine river in the upper right corner of the image. The deep learning method missed segments in regions C and E, and fine patches remained in regions B and C. The SVM method misclassified the edge of the large pond as an aquaculture pond. In contrast, the object-based + decision tree method proposed in this paper removed the thin river, the large pond, and other easily confused features; it demonstrated fewer missed segments and no fine patches. Therefore, our extraction results are superior and more efficient.

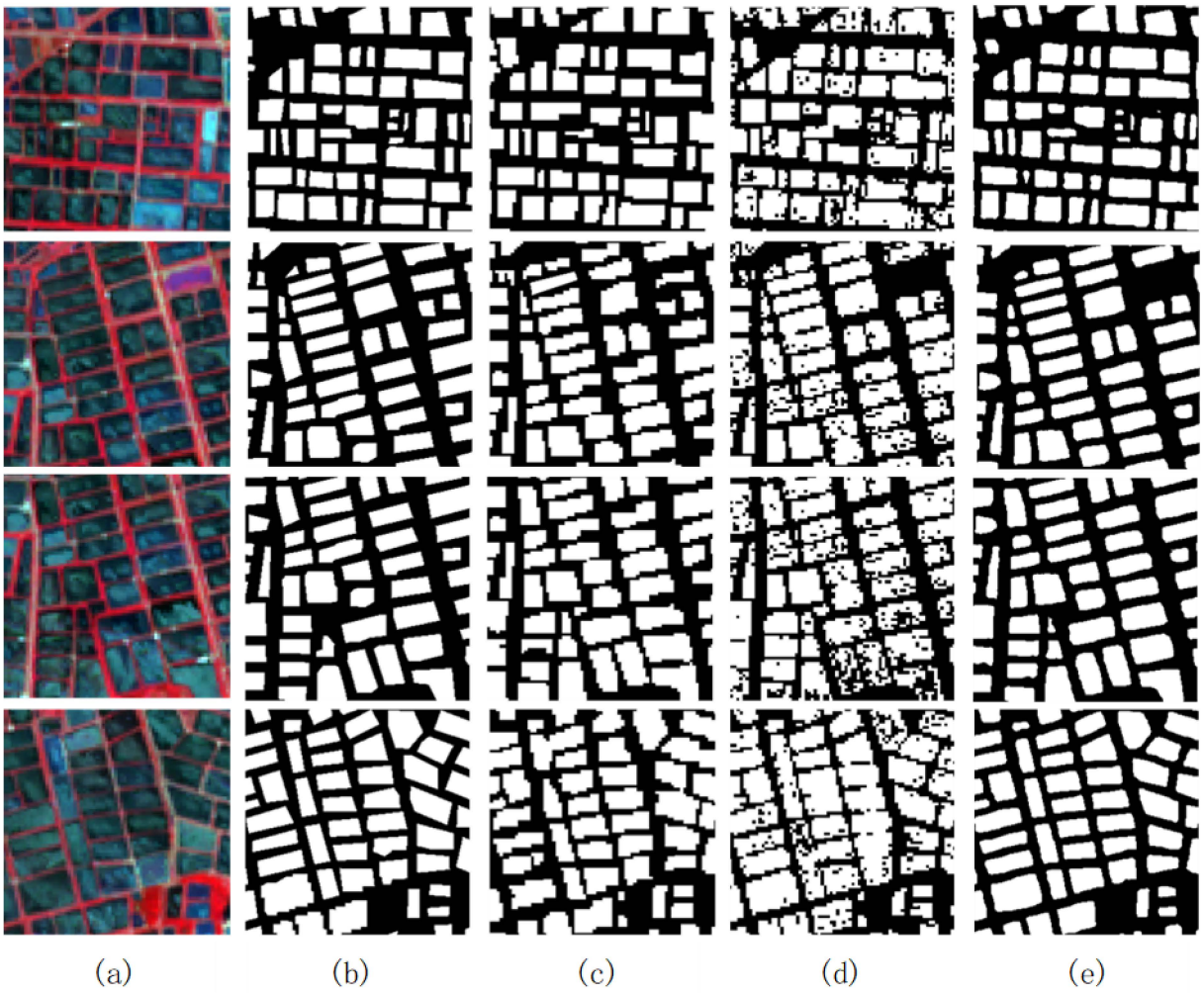

Figure 10. Comparison of extracted results. (**a**) Band combination 843; (**b**) label; (**c**) object-based + decision tree extraction results; (**d**) SVM extraction results; (**e**) deep learning extraction results.

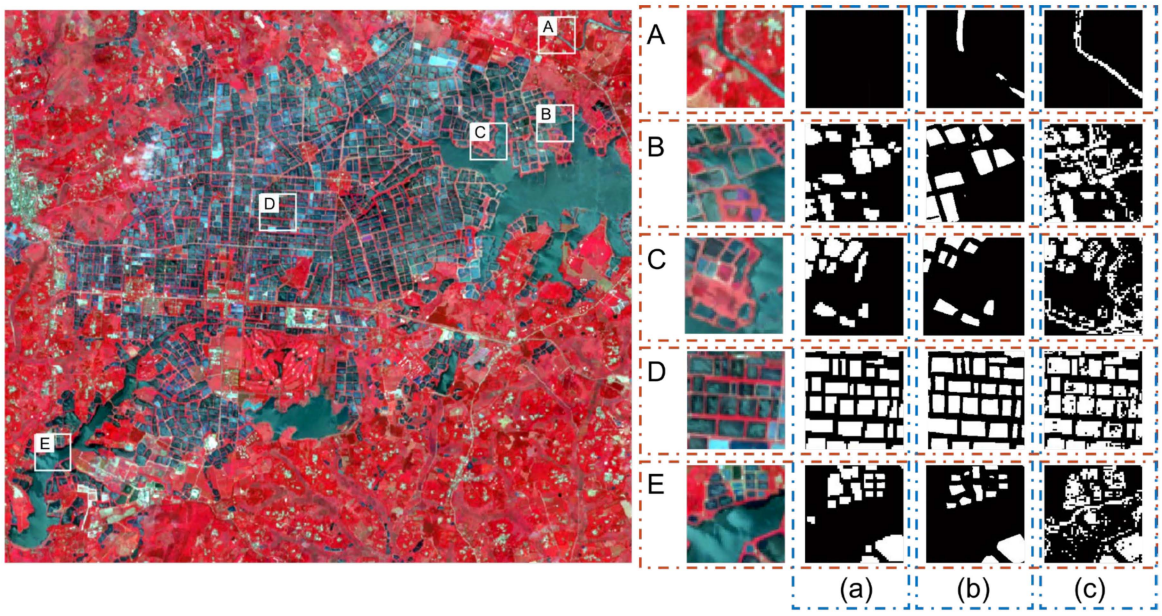

Figure 11. (**A**–**E**) Comparison of extracted results. (**a**) Object-based + decision tree; (**b**) deep learning; (**c**) SVM.

4. Discussion

4.1. The Analysis of the SVM Method

In comparing the extraction effects of the three methods, it is clear that the traditional machine learning method exhibited the lowest extraction accuracy, a serious misclassification phenomenon, the presence of "sticking", and too many small areas of impurity. This is primarily due to the fact that the method uses a single image element as the smallest classification unit and only considers the brightness value of the image element as a feature; it does not consider the spatial and shape characteristics of the ponds. In addition, this method requires the training samples to be drawn artificially, which is a strong subjective factor, and the extraction results rely heavily on the artificially drawn pieces.

4.2. The Analysis of the Deep Learning Method

The deep learning (U-Net) method exhibited the highest accuracy and can accurately extract ISAPs. The extracted ISAPs have complete boundaries. However, this method's extraction also resulted in some missed areas; it could not effectively eliminate fine river features, and tiny patches remained. Moreover, it is a data-dependent method, and the quality of the selected data has a great impact on the algorithm; in practice, this means that a large number of computational resources is required, including CPU, GPU, and the cloud server resources of local computers. Furthermore, its interpretability is poor, and the internal operating mechanism of the model is vague. Therefore, it is also difficult to troubleshoot and detect errors and bugs in this model, and it is difficult to prevent potential accidents from occurring. When conducting large-scale, fast, real-time, and dynamic aquaculture area mapping, the U-Net method takes a long time to accrue training data and may lack datasets that are relevant to the necessary research area, making it difficult to complete tasks.

4.3. The Analysis of the Object-Based + Decision Tree Method

The object-based + decision tree method proposed in this paper was shown to be more effective than the traditional machine learning method in terms of accuracy. The extracted aquaculture ponds have complete boundaries, and the phenomenon of "sticking together" was avoided. Compared with the deep learning method, it can distinguish ponds, rivers, and other features that are easily confused with aquaculture ponds. This is because our method utilizes image objects consisting of multiple adjacent image elements as extraction objects, thereby effectively avoiding the problems caused by small areas of impurity and incomplete pond boundaries that can occur within traditional machine learning methods. Moreover, we took into account characteristics other than brightness values that are unique to ponds, such as the compactness, area, aspect ratio, etc. In addition, we removed small rivers, pits, and ponds, and we segmented individual ponds. Our method is simple and quick to operate with limited samples. It does not depend on the quality of local computer hardware and requires few computational resources. We were able to see the extraction effect of each step of the decision tree in real time and then interpret the extraction results; errors within this extraction method were easy to troubleshoot. This method is also extremely efficient and can quickly map a large range of aquaculture areas with accuracy comparable to that of deep learning models. Furthermore, our method is lightweight, and modules can be added or removed at any time (depending on the extraction task). In summary, the object-based + decision tree method proposed in this paper is an ideal method of extracting extensive areas of aquaculture ponds.

4.4. Potential for Transferability

In order to test the transportability of our method, we selected areas of an aggregation of aquaculture ponds near the study area. The extraction results are shown in Figure 12. It can be seen that our method effectively eliminates non-water bodies and non-aquaculture water bodies such as puddles. In addition, our method also performs very well in removing dikes and can prevent most adhesion phenomena. However, due to the limited resolution

of our images and the fact that some embankments are too thin, some aquaculture ponds still show a little adhesion. We randomly generated 150 points on Google Earth, tested our extraction effect, and found that the accuracy rate was over 80%.

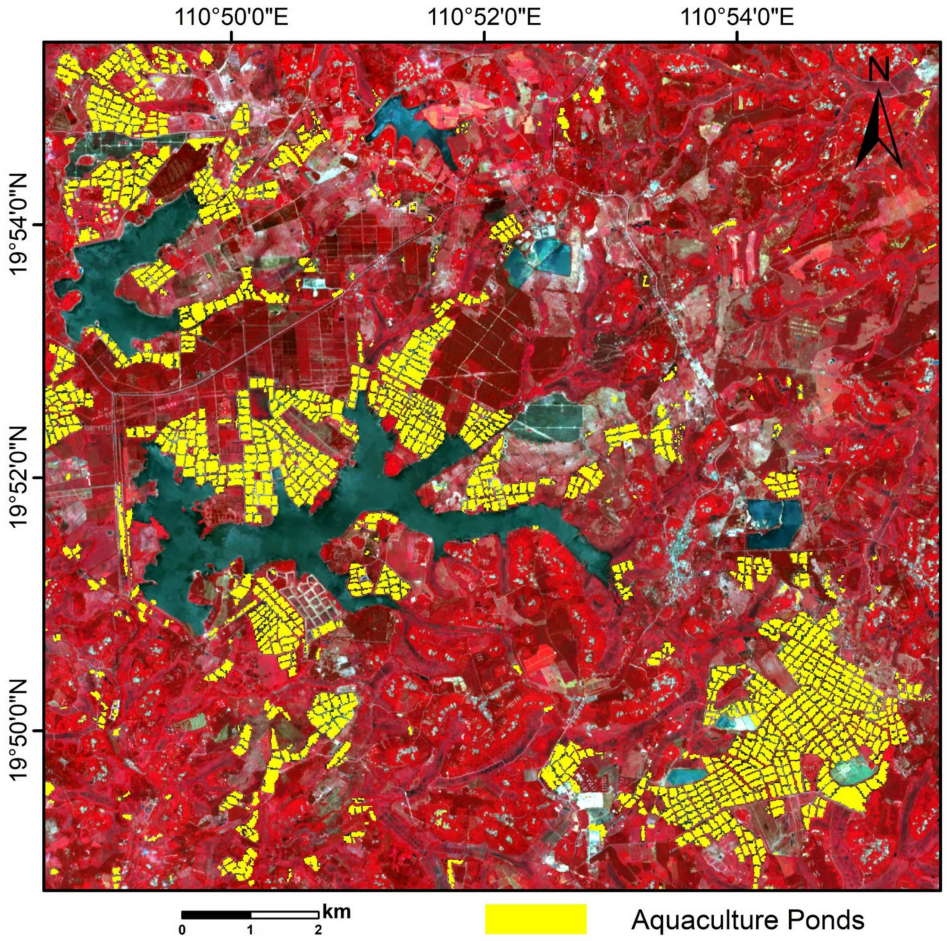

Figure 12. Algorithm transferability results.

5. Conclusions

Our research will aid the accurate extraction of ISAPs from Sentinel-2 images. In the context of the rapid expansion of aquaculture areas in China and the need to establish an efficient system for monitoring aquaculture areas, we proposed an object-based method from Sentinel-2 data. We used multi-scale segmentation to obtain water objects and then selected the NDWI index to initially separate land and water; finally, we built a decision tree based on expert knowledge to extract ISAPs. We tested the effects of traditional machine learning, deep learning, and our method. The three methods were discussed in detail, both quantitatively and qualitatively. The following conclusions were drawn from the 29 March 2024 results obtained in this study:

1. The proposed method can extract ISAPs with high accuracy; the accuracy (P) and recall (R) were around 85%, revealing that our method could effectively map aquaculture ponds.
2. The proposed method showed better performance than SVM and U-Net. Our method can avoid adhesion and extract ISAPs that have previously not been accurately omitted from different water bodies. It is easy to operate and does not depend on the quality of local computer hardware, so it is suitable for the real-time and rapid extraction of large aquaculture areas.

3. Our method has good transferability and can achieve an accuracy of more than 80% in the extraction of near-shore aquaculture ponds.

As it is an object-based algorithm, we were able to propose suitable application scenarios for this method. However, the same parameters may not be applicable when the scenarios are different, thus operators with professional knowledge will be required. We will further improve our method by modifying these adaptive thresholds in the hope of broadening its range of application scenarios.

Author Contributions: Conceptualization, Y.H. and L.Z.; methodology, Y.H. and B.C.; validation, Y.H. and J.Z.; formal analysis, Y.H.; investigation, Y.H. and J.Z.; data curation, Y.H.; writing—original draft preparation, Y.H.; writing—review and editing, Y.H., L.Z. and B.C.; visualization, Y.H.; supervision, L.Z.; project administration, Y.H. and B.C.; funding acquisition, B.C. All authors have read and agreed to the published version of the manuscript.

Funding: This research is supported by the Director Fund of the International Research Center of Big Data for Sustainable Development Goals, Grant No. CBAS2022DF003.

Data Availability Statement: The data presented in this study are available on request from the corresponding author.

Acknowledgments: The authors are very grateful to the anonymous reviewers for their valuable comments and suggestions for the improvement of this paper.

Conflicts of Interest: The authors declare no conflicts of interest.

References

1. Bank, M.S.; Metian, M.; Swarzenski, P.W. Defining Seafood Safety in the Anthropocene. *Environ. Sci. Technol.* **2020**, *54*, 8506–8508. [CrossRef] [PubMed]
2. Jiang, Q.; Bhattarai, N.; Pahlow, M.; Xu, Z. Environmental Sustainability and Footprints of Global Aquaculture. *Resour. Conserv. Recycl.* **2022**, *180*, 106183. [CrossRef]
3. Eswaran, H.; Lal, R.; Reich, P.F. Land degradation: An overview. In *Response to Land Degradation*; CRC Press: Boca Raton, FL, USA, 2019; pp. 20–35.
4. Karami, F.; Shotorbani, P.M. Genetically modified foods: Pros and cons for human health. *Food Health* **2018**, *1*, 18–23.
5. McFadden, B.R.; Lusk, J.L. What consumers don't know about genetically modified food, and how that affects beliefs. *FASEB J.* **2016**, *30*, 3091–3096. [CrossRef]
6. Yuan, J.; Xiang, J.; Liu, D.; Kang, H.; He, T.; Kim, S.; Lin, Y.; Freeman, C.; Ding, W. Rapid Growth in Greenhouse Gas Emissions from the Adoption of Industrial-Scale Aquaculture. *Nat. Clim. Chang.* **2019**, *9*, 318–322. [CrossRef]
7. Minahal, Q.; Munir, S.; Komal, W.; Fatima, S.; Liaqat, R.; Shehzadi, I. Global impact of COVID-19 on aquaculture and fisheries: A review. *Int. J. Fish. Aquat. Stud.* **2020**, *8*, 42–48.
8. Nasr-Allah, A.; Gasparatos, A.; Karanja, A.; Dompreh, E.B.; Murphy, S.; Rossignoli, C.M.; Phillips, M.; Charo-Karisa, H. Employment Generation in the Egyptian Aquaculture Value Chain: Implications for Meeting the Sustainable Development Goals (SDGs). *Aquaculture* **2020**, *520*, 734940. [CrossRef]
9. Food and Agriculture Organization (FAO). *The State of World Fisheries and Aquaculture 2022. Towards Blue Transformation*; FAO: Rome, Italy, 2022; ISBN 978-92-5-136364-5.
10. Wu, X.; Fu, B.; Wang, S.; Song, S.; Li, Y.; Xu, Z.; Wei, Y.; Liu, J. Decoupling of SDGs Followed by Re-Coupling as Sustainable Development Progresses. *Nat. Sustain.* **2022**, *5*, 452–459. [CrossRef]
11. Subasinghe, R.; Soto, D.; Jia, J. Global Aquaculture and Its Role in Sustainable Development. *Rev. Aquac.* **2009**, *1*, 2–9. [CrossRef]
12. Ren, C.; Wang, Z.; Zhang, Y.; Zhang, B.; Chen, L.; Xi, Y.; Xiao, X.; Doughty, R.B.; Liu, M.; Jia, M.; et al. Rapid expansion of coastal aquaculture ponds in China from Landsat observations during 1984–2016. *Int. J. Appl. Earth Obs. Geoinf.* **2019**, *82*, 101902. [CrossRef]
13. Liu, D.; Keesing, J.K.; Xing, Q.; Shi, P. World's largest macroalgal bloom caused by expansion of seaweed aquaculture in China. *Mar. Pollut. Bull.* **2009**, *58*, 888–895. [CrossRef] [PubMed]
14. Duan, Y.; Tian, B.; Li, X.; Liu, D.; Sengupta, D.; Wang, Y.; Peng, Y. Tracking changes in aquaculture ponds on the China coast using 30 years of Landsat images. *Int. J. Appl. Earth Obs. Geoinf.* **2021**, *102*, 102383. [CrossRef]
15. Bouslihim, Y.; Kharrou, M.H.; Miftah, A.; Attou, T.; Bouchaou, L.; Chehbouni, A. Comparing Pan- sharpened Landsat-9 and Sentinel-2 for Land-Use Classification Using Machine Learning Classifiers. *J. Geovis. Spat. Anal.* **2022**, *6*, 35. [CrossRef]
16. Yao, H. Characterizing landuse changes in 1990–2010 in the coastal zone of Nantong, Jiangsu province, China. *Ocean Coast. Manag.* **2013**, *71*, 108–115. [CrossRef]
17. Duan, Y.; Li, X.; Zhang, L.; Liu, W.; Chen, D.; Ji, H. Detecting spatiotemporal changes of large-scale aquaculture ponds regions over 1988–2018 in Jiangsu Province, China using Google Earth Engine. *Ocean Coast. Manag.* **2020**, *188*, 105144. [CrossRef]

18. Yao, Y.C.; Ren, C.Y.; Wang, Z.M.; Wang, C.; Deng, P.Y. Monitoring of salt ponds and aquaculture ponds in the coastal zone of China in 1985 and 2010. *Wetl. Sci.* **2016**, *14*, 874–882.
19. Zhang, L.; Zuo, J.; Chen, B.; Liao, J.; Yan, M.; Bai, L.; Sutrisno, D.; Hashim, M.; Al Mamun, M.M.A. Improved indicators for the integrated assessment of coastal sustainable development based on Earth Observation Data. *Int. J. Digit. Earth* **2024**, *17*, 2310082. [CrossRef]
20. Zuo, J.; Zhang, L.; Chen, B.; Liao, J.; Hashim, M.; Sutrisno, D.; Hasan, M.E.; Mahmood, R.; Sani, D.A. Assessment of coastal sustainable development along the maritime silk road using an integrated natural-economic-social (NES) ecosystem. *Heliyon* **2023**, *9*, e17440. [CrossRef]
21. Spalding, M.D.; Ruffo, S.; Lacambra, C.; Meliane, I.; Hale, L.Z.; Shepard, C.C.; Beck, M.W. The role of ecosystems in coastal protection: Adapting to climate change and coastal hazards. *Ocean Coast. Manag.* **2014**, *90*, 50–57. [CrossRef]
22. Duan, H.; Zhang, H.; Huang, Q.; Zhang, Y.; Hu, M.; Niu, Y.; Zhu, J. Characterization and environmental impact analysis of sea land reclamation activities in China. *Ocean Coast. Manag.* **2016**, *130*, 128–137. [CrossRef]
23. Tian, B.; Wu, W.; Yang, Z.; Zhou, Y. Drivers, trends, and potential impacts of long-term coastal reclamation in China from 1985 to 2010. *Estuar. Coast. Shelf Sci.* **2016**, *170*, 83–90. [CrossRef]
24. Liu, Y.; Wang, Z.; Yang, X.; Zhang, Y.; Yang, F.; Liu, B.; Cai, P. Satellite-based monitoring and statistics for raft and cage aquaculture in China's offshore waters. *Int. J. Appl. Earth Obs. Geoinf.* **2020**, *91*, 102118. [CrossRef]
25. Cheng, B.; Liang, C.; Liu, X.; Liu, Y.; Ma, X.; Wang, G. Research on a novel extraction method using Deep Learning based on GF-2 images for aquaculture areas. *Int. J. Remote Sens.* **2020**, *41*, 3575–3591. [CrossRef]
26. Fu, Y.; Deng, J.; Ye, Z.; Gan, M.; Wang, K.; Wu, J.; Yang, W.; Xiao, G. Coastal aquaculture mapping from very high spatial resolution imagery by combining object-based neighbor features. *Sustainability* **2019**, *11*, 637. [CrossRef]
27. Fu, Y.; Ye, Z.; Deng, J.; Zheng, X.; Huang, Y.; Yang, W.; Wang, Y.; Wang, K. Finer resolution mapping of marine aquaculture areas using worldView-2 imagery and a hierarchical cascade convolutional neural network. *Remote Sens.* **2019**, *11*, 1678. [CrossRef]
28. Ottinger, M.; Clauss, K.; Huth, J.; Eisfelder, C.; Leinenkugel, P.; Kuenzer, C. Time series sentinel-1 SAR data for the mapping of aquaculture ponds in coastal Asia. In Proceedings of the IGARSS 2018—2018 IEEE International Geoscience and Remote Sensing Symposium, Valencia, Spain, 22–27 July 2018.
29. Sun, Z.; Luo, J.; Gu, X.; Qi, T.; Xiao, Q.; Shen, M.; Ma, J.; Zeng, Q.; Duan, H. Policy-driven opposite changes of coastal aquaculture ponds between China and Vietnam: Evidence from Sentinel-1 images. *Aquaculture* **2023**, *571*, 739474. [CrossRef]
30. Ali, I.; Cao, S.; Naeimi, V.; Paulik, C.; Wagner, W. Methods to remove the border noise from Sentinel-1 synthetic aperture radar data: Implications and importance for time-series analysis. *IEEE J. Sel. Top. Appl. Earth Obs. Remote Sens.* **2018**, *11*, 777–786. [CrossRef]
31. Faqe Ibrahim, G.R.; Rasul, A.; Abdullah, H. Improving Crop Classification Accuracy with Integrated Sentinel-1 and Sentinel-2 Data: A Case Study of Barley and Wheat. *J. Geovis. Spat. Anal.* **2023**, *7*, 22. [CrossRef]
32. Wang, M.; Mao, D.; Xiao, X.; Song, K.; Jia, M.; Ren, C.; Wang, Z. Interannual changes of coastal aquaculture ponds in China at 10-m spatial resolution during 2016–2021. *Remote Sens. Environ.* **2023**, *284*, 113347. [CrossRef]
33. Wang, Z.; Zhang, J.; Yang, X.; Huang, C.; Su, F.; Liu, X.; Liu, Y.; Zhang, Y. Global mapping of the landside clustering of aquaculture ponds from dense time-series 10 m Sentinel-2 images on Google Earth Engine. *Int. J. Appl. Earth Obs. Geoinf.* **2022**, *115*, 103100. [CrossRef]
34. Shirani, K.; Solhi, S.; Pasandi, M. Automatic Landform Recognition, Extraction, and Classification using Kernel Pattern Modeling. *J. Geovis. Spat. Anal.* **2023**, *7*, 2. [CrossRef]
35. Diniz, C.; Cortinhas, L.; Pinheiro, M.L.; Sadeck, L.; Fernandes Filho, A.; Baumann, L.R.F.; Adami, M.; Souza-Filho, P.W.M. A large-scale deep-learning approach for multi-temporal aqua and salt-culture mapping. *Remote Sens.* **2021**, *13*, 1415. [CrossRef]
36. He, X.; Zhou, Y.; Zhao, J.; Zhang, D.; Yao, R.; Xue, Y. Swin transformer embedding UNet for remote sensing image semantic segmentation. *IEEE Trans. Geosci. Remote Sens.* **2022**, *60*, 4408715. [CrossRef]
37. Dang, K.B.; Nguyen, M.H.; Nguyen, D.A.; Phan, T.T.H.; Giang, T.L.; Pham, H.H.; Nguyen, T.N.; Tran, T.T.V.; Bui, D.T. Coastal wetland classification with deep u-net convolutional networks and sentinel-2 imagery: A case study at the tien yen estuary of Vietnam. *Remote Sens.* **2020**, *12*, 3270. [CrossRef]
38. Daw, A.; Karpatne, A.; Watkins, W.; Read, J.; Kumar, V. Physics-Guided Neural Networks (PGNN): An Application in Lake Temperature Modeling. *arXiv* **2021**, arXiv:1710.11431.
39. Moraffah, R.; Karami, M.; Guo, R.; Raglin, A.; Liu, H. Causal interpretability for machine learning-problems, methods and evaluation. *ACM SIGKDD Explor. Newsl.* **2020**, *22*, 18–33. [CrossRef]
40. Ottinger, M.; Clauss, K.; Kuenzer, C. Large-scale assessment of coastal aquaculture ponds with Sentinel-1 time series data. *Remote Sens.* **2017**, *9*, 440. [CrossRef]
41. Prasad, K.A.; Ottinger, M.; Wei, C.; Leinenkugel, P. Assessment of coastal aquaculture for India from Sentinel-1 SAR time series. *Remote Sens.* **2019**, *11*, 357. [CrossRef]
42. Loberternos, R.A.; Porpetcho, W.P.; Graciosa, J.C.A.; Violanda, R.R.; Diola, A.G.; Dy, D.T.; Otadoy, R.E.S. An object-based workflow developed to extract aquaculture ponds from airborne lidar data: A test case in central visayas, philippines. *Int. Arch. Photogramm. Remote Sens. Spat. Inf. Sci.* **2016**, *41*, 1147–1152. [CrossRef]
43. Ottinger, M.; Clauss, K.; Kuenzer, C. Opportunities and Challenges for the Estimation of Aquaculture Production Based on Earth Observation Data. *Remote Sens.* **2018**, *10*, 1076. [CrossRef]

44. Ottinger, M.; Bachofer, F.; Huth, J.; Kuenzer, C. Mapping aquaculture ponds for the coastal zone of Asia with Sentinel-1 and Sentinel-2 time series. *Remote Sens.* **2021**, *14*, 153. [CrossRef]
45. Yasir, M.; Sheng, H.; Fan, H.; Nazir, S.; Niang, A.J.; Salauddin, M.; Khan, S. Automatic coastline extraction and changes analysis using remote sensing and GIS technology. *IEEE Access* **2020**, *8*, 180156–180170. [CrossRef]
46. Su, T. Scale-variable region-merging for high resolution remote sensing image segmentation. *ISPRS J. Photogramm. Remote Sens.* **2019**, *147*, 319–334. [CrossRef]
47. Kolli, M.K.; Opp, C.; Karthe, D.; Pradhan, B. Automatic extraction of large-scale aquaculture encroachment areas using Canny Edge Otsu algorithm in Google Earth Engine–the case study of Kolleru Lake, South India. *Geocarto Int.* **2022**, *37*, 11173–11189. [CrossRef]
48. Li, Z.; Chen, J. Superpixel segmentation using linear spectral clustering. In Proceedings of the 2015 IEEE Conference on Computer Vision and Pattern Recognition (CVPR), Boston, MA, USA, 7–12 June 2015; pp. 1356–1363.
49. Yin, J.; Wang, T.; Du, Y.; Liu, X.; Zhou, L.; Yang, J. SLIC superpixel segmentation for polarimetric SAR images. *IEEE Trans. Geosci. Remote Sens.* **2021**, *60*, 5201317. [CrossRef]
50. Zhang, Y.; Liu, K.; Dong, Y.; Wu, K.; Hu, X. Semisupervised classification based on SLIC segmentation for hyperspectral image. *IEEE Geosci. Remote Sens. Lett.* **2019**, *17*, 1440–1444. [CrossRef]
51. Baatz, M.; Schäpe, A. Multiresolution segmentation—An optimization approach for high quality multi-scale image segmentation. In *Angewandte Geographische Informationsverarbeitung*; Strobl, J., Blaschke, T., Griesebner, G., Eds.; Wichmann-Verlag: Heidelberg, Germany, 2000; Volume 12, pp. 12–23.
52. Wang, J.; Jiang, L.; Wang, Y.; Qi, Q. An improved hybrid segmentation method for remote sensing images. *ISPRS Int. J. Geo-Inf.* **2019**, *8*, 543. [CrossRef]
53. Liu, F.; Lu, H.; Wu, L.; Li, R.; Wang, X.; Cao, L. Automatic Extraction for Land Parcels Based on Multi-Scale Segmentation. *Land* **2024**, *13*, 158. [CrossRef]
54. Zhang, F.B.; Yang, M.Y.; Li, B.B.; Li, Z.B.; Shi, W.Y. Effects of Slope Gradient on Hydro-Erosional Processes on an Aeolian Sand-Covered Loess Slope under Simulated Rainfall. *J. Hydrol.* **2017**, *553*, 447–456. [CrossRef]
55. Happ, P.N.; Ferreira, R.S.; Bentes, C.; Costa, G.A.O.P.; Feitosa, R.Q. Multiresolution Segmentation: A Parallel Approach for High Resolution Image Segmentation in Multicore Architectures. *Int. Arch. Photogramm. Remote Sens. Spat. Inf. Sci.* **2010**, *38*, C7.
56. Wang, X.; Niu, R. Landslide Intelligent Prediction Using Object-Oriented Method. *Soil Dyn. Earthq. Eng.* **2010**, *30*, 1478–1486. [CrossRef]
57. Drăguţ, L.; Eisank, C.; Strasser, T. Local variance for multi-scale analysis in geomorphometry. *Geomorphology* **2011**, *130*, 162–172. [CrossRef] [PubMed]
58. Drăguţ, L.; Tiede, D.; Levick, S. Esp: A tool to estimate scale parameters for multiresolution image segmentation of remotely sensed data. *Int. J. Geogr. Inf. Sci.* **2010**, *24*, 859–871. [CrossRef]
59. Drăguţ, L.; Csillik, O.; Eisank, C.; Tiede, D. Automated parameterisation for multi-scale image segmentation on multiple layers. *ISPRS J. Photogramm. Remote Sens.* **2014**, *88*, 119–127. [CrossRef]
60. Tong, X.; Luo, X.; Liu, S.; Xie, H.; Chao, W.; Liu, S.; Liu, S.; Makhinov, A.N.; Makhinova, A.F.; Jiang, Y. An approach for flood monitoring by the combined use of Landsat 8 optical imagery and COSMO-SkyMed radar imagery. *ISPRS J. Photogramm. Remote Sens.* **2018**, *136*, 144–153. [CrossRef]
61. Gstaiger, V.; Huth, J.; Gebhardt, S.; Wehrmann, T.; Kuenzer, C. Multi-sensoral and automated derivation of inundated areas using TerraSAR-X and ENVISAT ASAR data. *Int. J. Remote Sens.* **2012**, *33*, 7291–7304. [CrossRef]
62. Li, Z.; Zhang, X.; Xiao, P. Spectral index-driven FCN model training for water extraction from multispectral imagery. *ISPRS J. Photogramm. Remote Sens.* **2022**, *192*, 344–360. [CrossRef]
63. Work, E.A.; Gilmer, D.S. Utilization of satellite data for inventorying prairie ponds and lakes. *Photogramm. Eng. Remote Sens.* **1976**, *42*, 685–694.
64. Li, L.; Su, H.; Du, Q.; Wu, T. A novel surface water index using local background information for long term and large-scale Landsat images. *ISPRS J. Photogramm. Remote Sens.* **2021**, *172*, 59–78. [CrossRef]
65. Li, J.; Pei, Y.; Zhao, S.; Xiao, R.; Sang, X.; Zhang, C. A review of remote sensing for environmental monitoring in China. *Remote Sensing* **2020**, *12*, 1130. [CrossRef]
66. McFeeters, S.K. The use of the Normalized Difference Water Index (NDWI) in the delineation of open water features. *Int. J. Remote Sens.* **1996**, *17*, 1425–1432. [CrossRef]
67. Xu, H. Modification of normalised difference water index (NDWI) to enhance open water features in remotely sensed imagery. *Int. J. Remote Sens.* **2006**, *27*, 3025–3033. [CrossRef]
68. Nedkov, R. Orthogonal transformation of segmented images from the satellite Sentinel-2. *Comptes Rendus L'acad. Bulg. Sci.* **2017**, *70*, 687–692.
69. Guo, Q.; Pu, R.; Li, J.; Cheng, J. A weighted normalized difference water index for water extraction using Landsat imagery. *Int. J. Remote Sens.* **2017**, *38*, 5430–5445. [CrossRef]
70. Du, Z.; Linghu, B.; Ling, F.; Li, W.; Tian, W.; Wang, H.; Gui, Y.; Sun, B.; Zhang, X. Estimating surface water area changes using time-series Landsat data in the Qingjiang River Basin, China. *J. Appl. Remote Sens.* **2012**, *6*, 063609.
71. Du, Y.; Zhang, Y.; Ling, F.; Wang, Q.; Li, W.; Li, X. Water bodies' mapping from Sentinel-2 imagery with modified normalized difference water index at 10-m spatial resolution produced by sharpening the SWIR band. *Remote Sens.* **2016**, *8*, 354. [CrossRef]

72. Lu, S.; Wu, B.; Yan, N.; Wang, H. Water body mapping method with HJ-1A/B satellite imagery. *Int. J. Appl. Earth Obs. Geoinf.* **2011**, *13*, 428–434. [CrossRef]
73. Otsu, N. A threshold selection method from gray-level histograms. *IEEE Trans. Syst. Man Cybern.* **1979**, *9*, 62–66. [CrossRef]
74. Waske, B.; van der Linden, S.; Benediktsson, J.A.; Rabe, A.; Hostert, P.; Sensing, R. Sensitivity of support vector machines to random feature selection in classification of hyperspectral data. *IEEE Trans. Geosci. Remote Sens.* **2010**, *48*, 2880–2889. [CrossRef]
75. Zunair, H.; Ben Hamza, A. Sharp U-Net: Depthwise convolutional network for biomedical image segmentation. *Comput. Biol. Med.* **2021**, *136*, 104699. [CrossRef]